JOURNAL OF MATERIALS SCIENCE 22 (1987) 2859–2866

An investigation of atomic short range order in palladium alloys by diffraction methods

A. M. SHAMAH*, N. COWLAM, G. E. CARR‡
Department of Physics, University of Sheffield, Sheffield S3 7RH, UK

An investigation of the degree of atomic short range order (ASRO) in alloys of palladium with scandium, dysprosium, titanium and manganese has been made using X-ray and neutron diffraction. The feasibility of performing such experiments is first discussed and following this, a number of alloys with different compositions and heat treatments have been examined. Measurable ASRO has been observed only in the most favourable cases $Pd_{0.86}Ti_{0.14}$ and $Pd_{0.85}Mn_{0.15}$. The ASRO parameters have been determined for these examples and the form of the ASRO observed discussed in relation to long-range ordered phases.

1. Introduction

The strong affinities for gaseous atoms exhibited by certain transition metals is well known and has been responsible for the technological use of such metals in gas separation and gas storage devices. Metallurgical problems can sometimes hinder the straightforward application of such metals. In the palladium–hydrogen system, for example, a miscibility gap exists between two face-centred cubic phases designated α and β [1]. There is a 33% linear size difference between these phases [2], so that cycling palladium with hydrogen across the miscibility gap can lead to distortion and failure of thin specimens of palladium [3]. This makes pure palladium unsuitable for hydrogen separation membranes. In palladium–silver alloys, the miscibility gap is closed at room temperature at a critical concentration of 24% silver [4] and alloys beyond this concentration do not show distortion and failure on cycling [5].

Systematic studies over several years [6–11] have shown that palladium alloys with solutes other than silver–transition metal and rare earth solutes, may also exhibit favourable properties. This work has demonstrated, for instance, that the miscibility gap can be closed at significantly lower values of critical concentration $\sim 8\%$, for palladium alloys with europium, gadolinium and yttrium [7]. Effective diffusion membranes can be produced from $Pd_{0.92}Y_{0.08}$ and other alloys [8] and it has been pointed out that isotopic separation of hydrogen is possible using these palladium alloy membranes [11].

A suggestion arising from these measurements is that palladium alloys with compositions near to the critical value may have extensive atomic short range order (ASRO) between the constituents. This could have an important bearing on the hydrogen solubility and diffusity, since long range order has been shown to favour hydrogen solubility in intermetallic compounds with higher solute concentrations like Pd_3Fe [12] and Pd_3Mn [13]. It is not, however always easy to investigate this ASRO, which may be a precursor of a long range ordered state. Therefore, in several instances, the existence of ASRO has been inferred from, say, the variation of lattice parameter with composition and the relation between the lattice parameter values and those of the ordered phases [6]. Structures with *long-range* atomic order based on the stoichiometric composition Pd_3X are of course shown to exist for a wide variety of solutes [14].

The present investigation has concerned a diffraction study of ASRO in palladium-rich palladium–dysprosium, palladium–scandium, palladium–titanium and palladium–manganese alloys, using X-ray and neutron diffraction.

2. The visibility of ASRO in binary alloys of palladium

The ability to detect short or long-range order in a binary alloy depends obviously on the difference in the scattering amplitudes, ϕ, of the two species present. ϕ is the atomic scattering factor $f(Q)$ (and Q the scattering vector is $Q = 4\pi \sin\theta/\lambda$) for X-rays [15], or alternatively the nuclear scattering amplitude, b, for neutrons [16]. An estimate of the feasibility of diffraction experiments on palladium alloys can therefore be made prior to any actual measurements. The palladium–yttrium alloys above, are for example, rather poor candidates for diffraction work. Simple calculation of Bragg peak intensities shows that even for a completely (i.e. long-range) ordered Pd_3Y alloy, the superlattice Bragg peaks in the diffraction pattern are virtually at the limit of detection – of the order of 1% of the intensities of the fundamental Bragg peaks. Therefore intuitively, there is little chance of detecting the corresponding ASRO. A measure of the ability to see ASRO in palladium alloys can be derived from the magnitudes of the scattering amplitudes by using the

*Present address: Physics Department, College of Education, Abha, PO Box 938, Saudi Arabia.
‡Present address: Department of Metallurgy, University of Sheffield, Sheffield S1 3JD, UK.

0022–2461/87 $03.00 + .12

TABLE I The values of the ratio R, defined in the text as a measure of ASRO scattering, are given for a representative selection of palladium alloys having composition $Pd_{0.75}M_{0.25}$. The ratios relative to that for Pd_3Y, the alloy proposed for membrane fabrication are also given.

Alloy composition	Ratio R for ASRO scattering			
	X-rays		Neutrons	
	R_X	Relative R'_X	R_N	Relative R'_N
Pd_3Sc	0.069	14.7*	0.102	6.4*
Pd_3Ti	0.063	13.4*	0.554	34.9*
Pd_3Mn	0.047	10.1	0.571	35.9*
Pd_3Fe	0.043	9.1	0.046	2.9
Pd_3Zr	0.003	0.7	0.006	0.4
Pd_3In	0.001	0.2	0.027	1.7
Pd_3Ag	0.000	0.02	0.000	0
Pd_3Y	0.005	1.00	0.016	1.00
Pd_3Ce	0.011	2.3	0.008	0.5
Pd_3Eu	0.021	4.5	0.014	0.9
Pd_3Gd	0.023	5.0	0.002	0.1
Pd_3Tb	0.026	5.4	0.012	0.7
Pd_3Dy	0.028	6.0	0.226	14.2*
Pd_3Ho	0.031	6.5	0.026	1.6
Pd_3Er	0.033	7.0	0.016	1.0
Pd_3Tm	0.036	7.7	0.007	0.4
Pd_3Yb	0.038	8.2	0.122	7.7
Pd_3Lu	0.041	8.8	0.008	0.5

*Possible candidate for diffraction studies.

ratio

$$R = x(1 - x)(\phi_{Pd} - \phi_M)^2/\langle\phi^2\rangle \qquad (1)$$

for the binary alloy $Pd_{1-x}M_x$ where $\langle\phi^2\rangle = (1 - x)\phi^2_{Pd} + x\phi^2_M$. The numerator represents the Laue monotonic scattering about which the ASRO scattering oscillates, see below, and the denominator is related to the total scattering level. The ratio therefore indicates the fraction of scattering associated with ASRO. The values of this ratio have been calculated for a number of palladium alloys, see Table I. The X-ray values are for zero scattering vector where $f(0) = Z$ the atomic number, while for neutrons the values are independent of angle as the nuclear scattering is isotropic. The alloys are arranged in Table I in two groups around the important [8] palladium–silver and palladium–yttrium examples. It is interesting to see that with palladium–silver alloys the visibility of ASRO is essentially zero with *both* radiations so no information on ASRO in these alloys can be obtained – unless neutron diffraction experiments using special (silver) isotope enriched specimens were performed. The visibility is also poor with palladium–yttrium alloys with both radiations and these low values have been used as a standard representing unity, in the columns showing the *relative* visibility of ASRO in these palladium alloys. The table shows that palladium rare earth alloys [7] are, in general, poor candidates for diffraction work, with the possible exception of palladium–dysprosium alloys. It will be shown below that this present work has involved a progressively more detailed investigation of certain palladium alloys culminating in measurements of palladium–titanium and palladium–manganese specimens. This was because the ASRO scattering was less evident that expected and palladium–titanium and palladium–manganese alloys represent particularly favourable cases for the investigation of ASRO when neutron diffraction is used. This occurs because neutrons are scattered from titanium, manganese and certain other nuclei, by a resonant, as opposed to a potential, scattering process [16]. Such nuclei are assigned negative values of scattering amplitude, $b_{Ti} = -0.3438 \times 10^{-12}$ cm; $b_{Mn} = -0.373 \times 10^{-12}$ cm, because the normal 180° phase change which occurs with potential scattering is absent. Negative values of b maximize the numerator in the expression for R (Equation 1) so that there is an enhanced contrast between the species for palladium–titanium and palladium–manganese alloys. The values of the ratio R in Table I suggest that palladium–scandium, palladium–titanium, palladium–manganese and palladium–dysprosium alloys are appropriate candidates for diffraction work with neutrons and to a lesser extent palladium–scandium and palladium–titanium alloys with X-rays, (as marked *). The ratios given in Table I are for alloys at the $Pd_{0.75}M_{0.25}$ composition, so for alloys with less solute, the ratio falls according to the term $x(1 - x)$. In order to select the best compositions for diffraction work this factor and the critical concentration (7 to 12% solute) needed to close the $\alpha \rightarrow \beta$ miscibility gap must be considered.

3. Experimental method

The account of the experiments will be divided into three sections. The first deals with the experimental arrangements, the second with the exploratory measurements needed to assess the magnitude of the ASRO present in the samples and the third with the measurement and interpretation of ASRO in selected individual samples.

3.1. Sample preparation and diffraction experiments

The alloys specified were all produced by argon-arc melting of spectroscopically pure constituents and, as insignificantly small weight losses were recorded, the nominal starting compositions are given throughout. The alloys were examined in neutron diffraction as cylindrical ingots 1 cm diameter and 5 cm high, cut in two longitudinally to provide better heat transfer on quenching. This also provided a flat surface for the X-ray investigations in reflection geometry. All the diffraction experiments were made at room temperature.

The X-ray experiments were performed using a conventional Philips PW 1050 diffractometer either with Cu$K\alpha$ radiation $\lambda = 0.154$ nm, or with Mo$K\alpha$ radiation $\lambda = 0.0711$ nm plus a curved crystal (graphite) monochromator. In a typical experiment a range of scattering angles $5° < 2\theta < 165°$ was covered with a step length 0.1°, the step time being arranged to allow an experiment of ~22 h duration. The neutron measurements were made on both Curran and 10 H neutron diffractometers at Dido Reactor (25 MW) AERE Harwell, having incident beams with $\lambda = 0.137$ nm (or $\lambda = 0.0995$ nm) and $\lambda = 0.104$ nm respectively. These instruments have five and three

neutron detectors respectively on a single arm, which may be programmed to move, say, $4° < 2\theta < 124°$ in 0.1° steps again over a 22 h period. The diffraction patterns are then constructed from the amalgamation of these three or five counter outputs.

Although the scattering mechanisms and the contributions to the total scattering are different with X-radiation and neutrons, the overall appearance of the diffraction patterns is similar for both radiations. The difference lies in the analysis of long range order and atomic short range order scattering. A completely disordered solid solution gives the "fundamental" Bragg peaks alone and an alloy with complete long range atomic order the additional "superlattice" peaks. These may be isolated from the (usually) smooth background scattering level and relative peak intensity measurements made to identify the structure present. An alloy with ASRO gives diffuse, but Q-dependent, background scattering (and usually the "fundamental" peaks) so that an absolute intensity measurement is necessary to isolate the true ASRO scattering from other contributions to the background. The observed scattering must first be corrected for instrumental background, absorption, incoherent scattering and, for neutrons, multiple scattering and inelastic scattering effects (Placzek corrections) are also important. These corrections have been comprehensively described by Moser *et al.* [17]. The ASRO scattering may then be isolated. With neutrons, the average level of the ASRO intensity may also be compared with that from a standard vanadium sample which scatters only incoherently and for which the (absolute) value of scattering cross-section is accurately known. Computer programs for these manipulations are well established [17, 18].

The ASRO scattered intensity, per atom, observed in a neutron diffraction experiment can be expressed (using a simple modification of the equations given by Warren [19] for the X-ray case) as a sum over i shells of neighbours each containing c_i neighbours a distance r_i away.

$$I_{\mathrm{ASRO}}(Q) = x(1 - x)(b_{\mathrm{Pd}} - b_{\mathrm{M}})^2 \sum_{i=0}^{\infty} c_i \alpha_i \frac{\sin Qr_i}{Qr_i} \tag{2}$$

Equation 2 is for an alloy $Pd_{1-x}M_x$ where b's are the nuclear scattering amplitudes. The α_i are the Cowley ASRO parameters [20]

$$\alpha_i = 1 - pr_i(\mathrm{M/Pd})/(1 - x) \tag{3}$$

where $pr_i(\mathrm{M/Pd})$ is the probability of finding a palladium atom in the ith neighbour shell around an M atom. The ASRO sum over shells can be replaced by an integral over an ASRO function $g(r)$ [19]

$$\sum_{i=0}^{\infty} c_i \alpha_i \frac{\sin Qr_i}{Qr_i} = \int_0^{\infty} g(r) \frac{\sin Qr}{Qr} \, \mathrm{d}r = j(Q) \tag{4}$$

so

$$I(Q) = x(1 - x)(b_{\mathrm{Pd}} - b_{\mathrm{M}})^2[1 + j(Q)] \tag{5}$$

and $g(r)$ can be determined by the Fourier transform of $j(Q)$ (which, as shown above, is derived from the experimentally measured intensity $I_{\mathrm{ASRO}}(Q)$) using Equation 5

$$g(r) = \frac{2}{\pi} \int_0^{Q_{\max}} Qj(Q) \sin QrM(Q) \, \mathrm{d}Q \tag{6}$$

Here $M(Q)$ is a "modification function" to allow for the non-infinite limit of the integral to the experimental value $Q_{\max}$. The value $g(r)$ differs from zero at radial values corresponding to the shell radii r_i of the crystalline structure under examination. Positive and negative peaks show like and unlike atomic corrections respectively. The area in each peak is equal to the product $c_i\alpha_i$, for that shell of neighbours

$$\int_{i\,\mathrm{th\,peak}} g(r) \, \mathrm{d}r = c_i\alpha_i \tag{7}$$

3.2. Preliminary measurements $Pd_{0.875}Sc_{0.125}$, $Pd_{0.90}Dy_{0.10}$, $Pd_{0.93}Ti_{0.07}$

Initially three alloys near to the critical concentration to close the $\alpha \rightarrow \beta$ miscibility gap [7] were prepared, $Pd_{0.875}Sc_{0.125}$, $Pd_{0.9}Dy_{0.1}$ and $Pd_{0.93}Ti_{0.07}$, and examined by neutron and X-ray diffraction. The following quenching and annealing treatments were given in order to try and induce observable ASRO. The samples were sealed in quartz tubes under a half an atmosphere of argon during all of these heat treatments and the quartz tubes were broken open at the moment of quench.

(a) Homogenized at 900° C for 24 h → quenched into cold water.

(b) Homogenized at 900° C for 2 h → furnace cooled to 300° C → annealed at 300° C for 12 h → furnace cooled to room temperature.

(c) Homogenized at 1100° C for 4 h → furnace cooled to 300° C → annealed at 300° C for 336 h → furnace cooled to room temperature.

In each case diffraction experiments showed that these alloys had the α-palladium face-centred cubic structure with the following lattice constants $Pd_{0.875}Sc_{0.125}$, $a = 0.3912$ nm; $Pd_{0.90}Dy_{0.10}$, $a = 0.3988$ nm; $Pd_{0.93}Ti_{0.07}$, $a = 0.3876$ nm. The alloys were found to be in the form of disordered solid solutions and no evidence of ASRO scattering was found. Fig 1 is a typical diffraction pattern for $Pd_{0.93}Ti_{0.07}$ after heat treatment (b) above, and shows the fundamental peaks of the face-centred cubic unit cell, no super lattice peaks, nor any oscillations about the Laue monotonic scattering.

3.3. Systematic investigations of $Pd_{1-x}Sc_x$ alloys

Following these measurements and the failure to observe ASRO in the specimens, palladium–scandium alloys were chosen, in view of the substantial body of previous work on these [6, 21, 22], for a more systematic diffraction investigation. An alloy $Pd_{0.75}Sc_{0.25}$ (Pd_3Sc) was produced first and examined by X-ray diffraction after the following quenching treatments:

(d) Homogenized at 900° C for 4 h → 1100° C for 2 h → quenched into cold water.

(e) Homogenized at 900° C for 4 h → quenched into cold water.

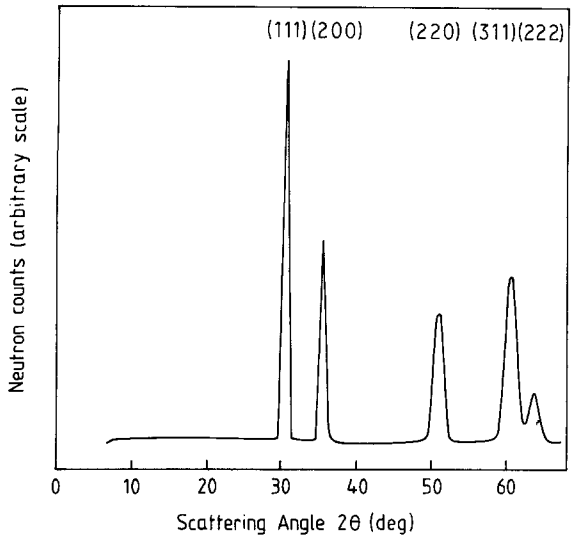

Figure 1 The neutron diffraction pattern for a $Pd_{0.93}Ti_{0.07}$ alloy given heat treatment (b), specified in the text, is shown. The Miller indices of the "fundamental" Bragg peaks are given in the top of the figure.

This alloy was found to have the $AuCu_3$ superlattice structure, with a unit cell dimension $a = 0.3962 \pm 0.0002$ nm similar to the values reported $a = 0.395\,79$ nm [6] and $a = 0.3973$ nm [22], while the long range order parameter was found to be close to unity $S = 0.928$. Having verified this strong tendency to order at the Pd_3Sc composition, a series of alloys $Pd_{1-x}Sc_x$ with $x = 0.23$, 0.20, 0.175, 0.15, 0.14 and subsequently $x = 0.165$ were produced. These were all given uniform heat treatments of

(f) Homogenized at 900° C for 72 h → quenched into cold water.

These alloys were examined by X-ray diffraction. The results of the investigation are summarised in Table II, which shows that a long range ordered (Cu_3Au) state was found in alloys $x = 0.25$, $x = 0.23$, $x = 0.20$, $x = 0.175$, while the alloys with $x = 0.15$ (and $x = 0.125$, as before) were found to have a disordered solid solution with no evidence of ASRO scattering to the limits of detection. An alloy of composition $Pd_{0.835}Sc_{0.165}$ was prepared and given the same heat treatment, (c) above. The X-ray diffraction pattern showed only a very weak (1 1 0) superlattice peak superimposed on a slightly sloping background, indicating the onset of the long range ordered state, with some small amount of ASRO present.

TABLE II Unit cell dimensions and the type of order present are specified for the series of Pd–Sc alloys examined by X-ray diffraction

Alloy composition	Unit cell dimension (nm)	Atomic arrangement
$Pd_{0.875}Sc_{0.125}$	0.3912	disordered solid solution
$Pd_{0.86}Sc_{0.14}$	0.3918	disordered solid solution
$Pd_{0.85}Sc_{0.15}$	0.3925	disordered solid solution
$Pd_{0.835}Sc_{0.165}$	0.3930	1 1 0 superlattice peak only
$Pd_{0.825}Sc_{0.175}$	0.3934	Superlattice peaks LRO present
$Pd_{0.80}Sc_{0.20}$	0.3948	Superlattice peaks LRO present
$Pd_{0.77}Sc_{0.23}$	0.3954	Superlattice peaks LRO present
$Pd_{0.75}Sc_{0.25}$	0.3962	LRO LI_2 type S = 0.928

The conclusion of similar measurements on these alloys by Norman and Harris [6] was that long range order was established for scandium concentrations greater than 0.175 and that no clearly defined two-phase region existed between the disordered and the long range ordered states. The present value of concentration for the onset of long range order ~0.165 is similar and the present measurements indicate that the ASRO in these palladium–scandium alloys must exist over only a narrow composition range about this figure.

3.4. Measurement of ASRO in palladium–titanium and palladium–manganese

Following the two exploratory investigations described in the previous sections, a final attempt to measure ASRO scattering in palladium-based alloys was made by neutron diffraction. Four alloys were chosen having compositions for which the previous measurements had indicated ASRO might occur, $Pd_{0.86}Dy_{0.14}$, $Pd_{0.86}Sc_{0.14}$ and the two particularly favourable cases (Table I) $Pd_{0.86}Ti_{0.14}$ and $Pd_{0.85}Mn_{0.15}$. The four alloys were given the heat treatment.

(g) Homogenized at 900° C for 48 h → quenched into cold water

and the neutron diffraction pattern of each obtained. The patterns of the palladium–scandium and palladium–dysprosium specimens contained just the fundamental Bragg peaks with no evidence of ASRO, but the more favourable palladium–titanium and palladium–manganese cases showed both the fundamental peaks and oscillating background levels indicative of ASRO. The positions of the fundamental peaks were recorded and the structure type and lattice parameter values obtained, $Pd_{0.86}Ti_{0.14}$, fcc, $a = 0.3881$ nm and $Pd_{0.85}Mn_{0.15}$, fcc, $a = 0.3887$ nm. These Bragg peaks were then removed from the diffraction pattern to allow an analysis of the ASRO scattering to be made in the manner explained in section 3.1. An additional correction was necessary for the $Pd_{0.85}Mn_{0.15}$ alloy which was paramagnetic and exhibited strong magnetic neutron scattering from the manganese atoms which carry a moment of $\mu = 4.5\,\mu_B$ (μ_B = Bohr magneton) [23]. The intensity per atom for this contribution can be written [16]

$$I(Q) = x\tfrac{2}{3}[p^2(Q)] \qquad (8)$$

where the magnetic scattering amplitude $p(Q) = 0.267 \times 10^{-12}\,\mu f(Q)$ cm, with $f(Q)$ the magnetic form factor and the numerical constant is $e^2\gamma/2mc^2$ [16]. The magnetic contribution accounted for approximately 31% of the total intensity at $Q = 0$. Figs 2 and 3 show the normalized ASRO intensity distributions for the two samples. The two curves have rather similar characteristics, a first peak at $Q_1 \sim 18.0$–$19.0\,\text{nm}^{-1}$,

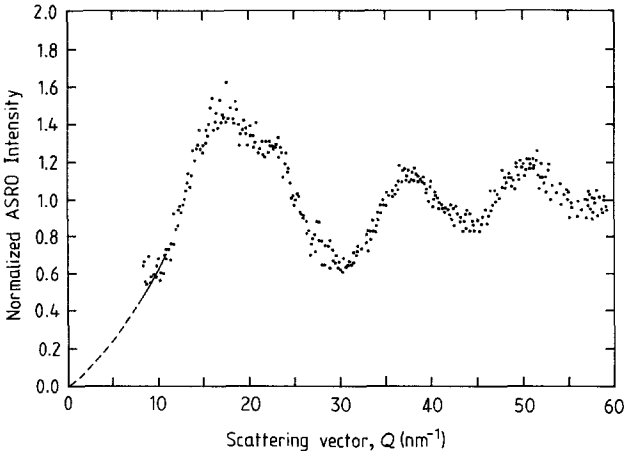

Figure 2 The normalized ASRO intensity curve for the $Pd_{0.86}Ti_{0.14}$ specimen is given as a function of scattering vector Q ($4\pi \sin\theta/\lambda$). Normalized ASRO intensity: $I(Q)/[0.14 \times 0.18(b_{Pd} - b_{Ti})^2] = [1 + j(Q)]$.

a second $Q_2 \sim 38.0$–39.0 nm and a third, which is less well developed for the $Pd_{0.85}Mn_{0.15}$ specimen. Although the statistical reliability of the curve for $Pd_{0.85}Mn_{0.15}$ is worse than that for $Pd_{0.86}Ti_{0.14}$ the oscillations in the former curve are slightly more strongly developed. The half widths of the first peak are similar for the two specimens $\Delta Q_1 = 9.4\,nm^{-1}$ for $Pd_{0.86}Ti_{0.14}$ and $\Delta Q_1 = 9.0\,nm^{-1}$ for $Pd_{0.85}Mn_{0.15}$. This suggests a characteristic range of correlated ASRO $r \sim 2\pi/\Delta Q_1 \sim 0.6$–$0.7$ nm.

4. Atomic short range order in $Pd_{0.85}Ti_{0.14}$ and $Pd_{0.85}Mn_{0.15}$ alloys

The $g(r)$ curves describing the ASRO in real space, derived from the Fourier transforms of the $j(Q)$ shown in Figs 2 and 3 are given in Figs 4a and 5a respectively.

The width of the peaks in $g(r)$ is a consequence of the finite limit of the integration in Equation 6 and to some extent the use of the modification function $M(Q)$. The characteristic resolution is given by $\Delta r \approx 2\pi/Q_{max} \approx 0.1$ nm which is commensurate with the observed peak widths. The positive and negative peaks in $g(r)$ must correspond to actual interatomic distances r_i in the face-centred cubic structures, calculated from the unit cell dimensions (see Table III)

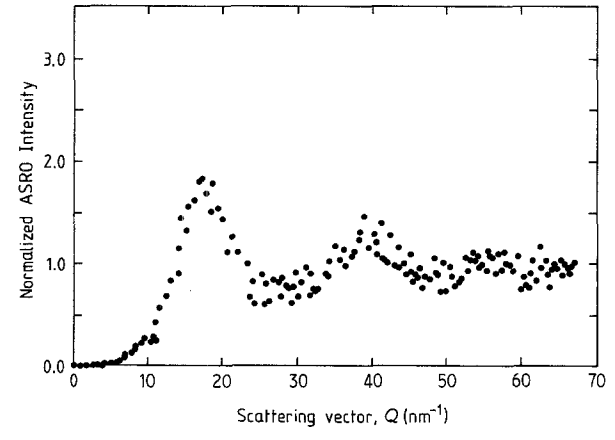

Figure 3 The normalized ASRO intensity curve for the $Pd_{0.85}Mn_{0.15}$ specimen. Normalized ASRO intensity; $I(Q)/[0.15 \times 0.85(b_{Pd} - b_{Mn})^2] = [1 + j(Q)]$.

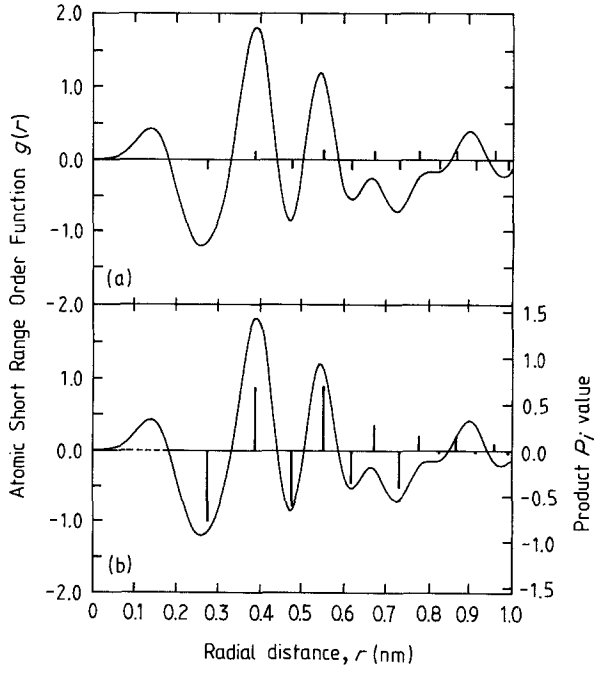

Figure 4 The ASRO function $g(r)$ for the $Pd_{0.86}Ti_{0.14}$ specimen derived from the Fourier transforms of the $j(Q)$ curve shown in Fig. 2 is given. In Fig. 4a the radial distances r_i to the successive shells are shown by the short vertical lines. In Fig. 4b the idealized ASRO based on a Cu_3Au type order is illustrated by the vertical lines proportional to the product P_i and specified in Table IV.

and shown by the short vertical lines in Figs 4 and 5. The reason these are drawn alternatively on either side of the abscissa is explained below. The $g(r)$ curves for both samples give evidence of true ASRO – a negative first peak indicative of unlike neighbours.

In the $g(r)$ curve for $Pd_{0.86}Ti_{0.14}$ the first hump is most probably an artifact of the Fourier transform (since no scientific basis existed for altering the normalization process, no attempt was made to minimise or remove the peak). Beyond this hump the correlation between peaks in $g(r)$ and the interatomic distances is good out to about 0.8–0.9 nm. ASRO

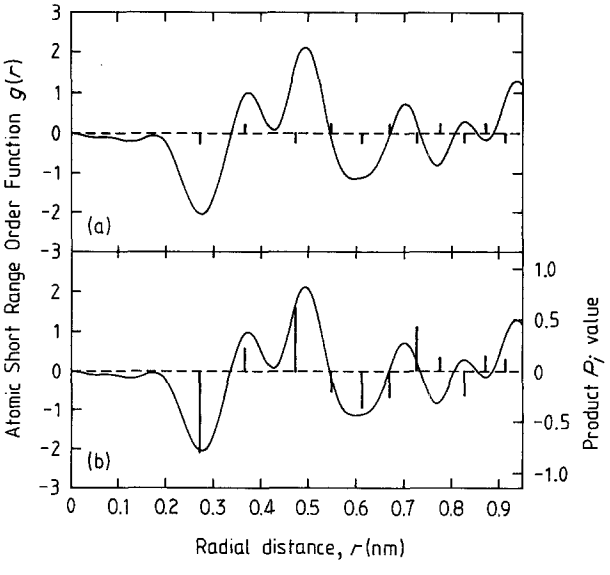

Figure 5 The ASRO function $g(r)$ for the $Pd_{0.85}Mn_{0.15}$ specimen is shown. Fig. 4a shows the distances to the atomic shells and Fig. 4b idealized ASRO based on the structural arrangement shown in Fig. 6 and specified in Table IV.

TABLE III The ASRO parameters and the occupation numbers for the shells of atoms obtained from the $g(r)$ curves of Figs 4a and 5a are given

Alloy	ASRO Parameters			Atomic occupation about a titanium or manganese origin			
	Shell number i	c_i	α_i	Random		Observed	
				n_{Pd}	n_{Ti}	n_{Pd}	n_{Ti}
$Pd_{0.86}Ti_{0.14}$	1	12	−0.094	10.3	1.7	11.3	0.7
	2	6	+0.162	5.2	0.8	4.3	1.7
	3	24	−0.013	20.6	3.4	20.9	3.1
	4	12	+0.050	10.3	1.7	9.8	2.2
				n_{Pd}	n_{Mn}	n_{Pd}	n_{Mn}
$Pd_{0.85}Mn_{0.15}$	1	12	−0.148	10.2	1.8	11.7	0.3
	2	6	+0.077	5.1	0.9	4.7	1.3
	3	24	+0.053	20.4	3.6	19.3	4.7
	4	12	~0.0	10.2	1.8	10.2	1.8
	5	24	−0.045	20.4	3.6	21.3	2.7

parameters can be obtained from the first four well-defined peaks in $g(r)$, and are given together with the site occupations in Table III. There are no spurious details in the $g(r)$ curve for the $Pd_{0.85}Mn_{0.15}$ alloy at small radial distances, but the peaks in $g(r)$ do not appear to correspond so clearly with the appropriate r_i values (see Fig. 5a) and the sequence of negative and positive peaks evident in Fig. 4a is absent. Nevertheless the ASRO parameters can be obtained for the first five r_i values and these are also given in Table III.

It is interesting to establish whether the observed ASRO in the two cases is the precursor of a fully long range ordered structure. This can be done as follows. Cowley has shown [20, 24] that limiting values of the α_i, say α_i^{lim} can be defined for perfectly ordered phases. The products $c_i\alpha_i^{lim}$ can then give an indication of the most highly developed ASRO that is possible for a particular structure. However account must also be taken of the range of ASRO in the real alloys. It has been suggested that the α_i may vary with distance according to the relations [25].

$$\alpha_i = \frac{\exp(-Ar_i)}{r_i} \tag{9}$$

Thus where A is a constant the product P_i can be used

$$P_i = \frac{c_i\alpha_i^{lim}\exp(-Ar_i)}{r_i} \tag{10}$$

to illustrate how a tendency to long range order can manifest itself, by means of ASRO with the appropriate range. This is done by drawing vertical lines with magnitudes equal to P_i and sign determined by α_i^{lim} at each of the r_i values of the atomic shells, see Figs 4b and 5b and Table IV. The characteristic range of the ASRO observed here can be accounted for with $A \sim 0.224$ in Equation 9 so that $\exp(-Ar)/r$ falls to about 0.01 for $r \sim 0.1$ nm.

The choice of a long range ordered structure as a prototype for the ASRO in $Pd_{0.86}Ti_{0.14}$ is made difficult by the disagreements which occur, for palladium concentrations greater than about 60%, between the existing palladium–titanium phase diagrams [26, 27]. It is not clear for example over what composition ranges Pd_4Ti, Pd_3Ti and Pd_2Ti structures may exist. A simple choice of a structure prototype is therefore a hypothetical Pd_3Ti fcc structure having long range order of the Cu_3Au ($L1_2$) type. (see Fig. 5). This is suggested by the regular negative to positive

TABLE IV Atomic shell parameters and the limiting values of α_i^{lim} are given for the Cu_3Au and AF3 ordered phases in the face-centred cubic system. The products P_i illustrated in Figs 4b and 5b are also listed

Shell parameters for fcc phase				Parameters for Cu_3Au LI_2 phase		Parameters for "AF3" phase	
Shell number	Cell co-ordinates	Interatomic distance r_i	Co-ordination No c_i	α_i^{lim}	P_i	α_i^{lim}	P_i
1	$\frac{1}{2}\frac{1}{2}0$	$a/\sqrt{2}$	12	−0.333	−0.788	−0.333	−0.786
2	100	a	6	1.0	0.648	0.333	0.215
3	$1\frac{1}{2}\frac{1}{2}$	$\sqrt{3/2}\,a$	24	−0.333	−0.581	0.333	0.578
4	110	$\sqrt{2}\,a$	12	1.0	0.639	−0.333	−0.212
5	$\frac{3}{2}\frac{1}{2}0$	$\sqrt{5/2}\,a$	24	−0.333	−0.330	−0.333	−0.329
6	111	$\sqrt{3}\,a$	8	1.0	0.264	−1.0	−0.263
7	$\frac{3}{2}1\frac{1}{2}$	$\sqrt{7/2}\,a$	48	−0.333	−0.433	0.333	0.432
8	200	2a	6	1.0	0.136	1.0	0.135
9	$\frac{3}{2}\frac{3}{2}0$ $(2\frac{1}{2}\frac{1}{2})$	$\sqrt{9/2}\,a$	36	−0.333	−0.023	−0.333	−0.299
10	$\frac{2}{3}\frac{1}{3}0$	$\sqrt{5}\,a$	24	1.0	0.395	0.333	0.131
11	$\frac{3}{2}\frac{3}{2}1$	$\sqrt{11/2}\,a$	24	−0.333	−0.114	0.333	0.114
12	211	$\sqrt{6}\,a$	24	1.0	0.288	–	–
13	$\frac{5}{2}\frac{1}{2}0$ $(2\frac{3}{2}1)$	$\sqrt{13/2}\,a$	24	−0.333	−0.088	–	–

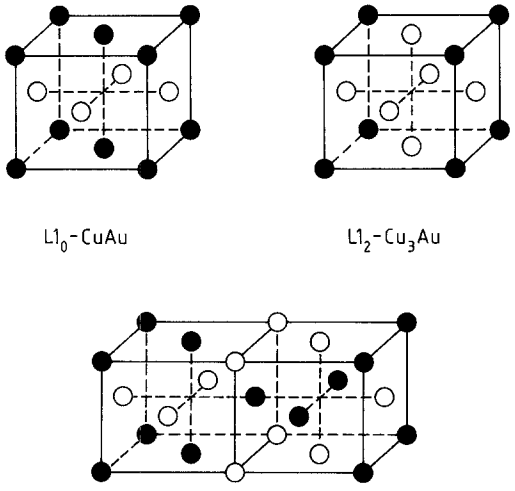

Figure 6 The CuAuI ($L1_0$) and Cu_3Au ($L1_2$) structures are shown in the top of the figure. At the bottom the equiatomic ordered arrangement [30] derived from the CuAuI structure and the analogue of the AF3 antiferromagnetic structure is shown.

oscillations in the $g(r)$ curve, Fig. 4a, because Cowley has shown [24] the limiting values for this phase are $\alpha_{even}^{lim} = 1.0$ and $\alpha_{odd}^{lim} = -0.333$.

The result of calculating the products P_i and superimposing appropriate lines on the $g(r)$ curve as described above, is shown in Fig. 4b, where the arbitrary scale of the P_i's is chosen to provide the best overall match with $g(r)$. The agreement between this simulation and the $g(r)$ curve is remarkably good.

The phase diagram for the palladium–manganese system [27] shows that there are no palladium-rich ordered phases and the palladium solid solution is separated by narrow two-phase regions from particularly stable phases in the equiatomic region which may be possible prototypes for the ASRO in $Pd_{0.85}Mn_{0.15}$. β-MnPd exists between 550° C and 1515° C but is unlike the palladium-rich alloys in having a bcc structure (CsCl type), while β_1-MnPd has a partially ordered version of the Cu_3Au structure, as discussed in [18]. Cowley has shown [20] that the equiatomic CuAu I fcc structure has, like Cu_3Au, limiting values α_i^{lim} which oscillate regularly, $\alpha_{even}^{lim} = 1.0$ and $\alpha_{odd}^{lim} = -0.333$, so it can be seen from Fig. 5a that neither of these structures represents an appropriate choice. Fortunately it has not been necessary to evaluate the α_i^{lim} values for myriad ordered phases to find a structure prototype for the ASRO in $Pd_{0.85}Mn_{0.15}$, since earlier work by us on equivalent magnetic systems [18] has identified an antiferromagnetic structure which has the right characteristics. This is the Type 3 antiferromagnetic structure (AF3) in the fcc phase [28]. The geometry of this and other antiferromagnetic structures has been specified by Darby and Webster [29]. In such antiferromagnetic structures the upwards and downwards directed magnetic moments correspond to A and B (palladium and M) atoms of a binary alloy – and the composition is always equiatomic. It is possible to use the data of Darby and Webster [29] to evaluate the α_i^{lim} values of the atomically ordered alloy equivalent to the AF3 structure. The values are given in Table III together with the products P_i and the structure is shown in Fig. 5. The P_i lines are superimposed on the $g(r)$ curve in Fig. 6b. Although the overall agreement is probably not as good as that for $Pd_{0.86}Ti_{0.14}$ the unusual sequence of negative and positive peaks in $g(r)$ is represented reasonably well out to the characteristic distance 0.6–0.7 nm.

5. Conclusion

It was the intention at the outset of this study to use X-ray diffraction to establish the broad features of ASRO in these palladium alloys and to optimise specimens for the more expensive neutron diffraction work. In the event, the experiments have shown that only in the most favourable cases has it been possible to make quantitive measurements of ASRO. In the absence of more complete and comprehensive neutron measurements on these palladium–titanium and palladium–manganese alloys our main conclusions must therefore be drawn from the stages of the present investigation as follows.

(a) It has not been possible to observe ASRO in alloys of palladium with scandium, dysprosium and titanium having compositions close to the critical concentration needed to close the $\alpha \rightarrow \beta$ miscibility gap, with either X-ray or neutron diffraction.

(b) Systematic measurements on palladium–scandium alloys have shown that measurable ASRO may occur in a relatively narrow composition range prior to the onset of a long range ordered state. This is supported by (c).

(c) ASRO has been detected and measured by neutron diffraction in the favourable cases of $Pd_{0.86}Ti_{0.14}$ and $Pd_{0.85}Mn_{0.15}$ alloys.

The ASRO parameters for these latter cases have been determined for the first four neighbour shells. The ASRO is not strongly established – the α_i values are never more than 28% and 44% of their maximum values for the $Pd_{0.86}Ti_{0.14}$ and $Pd_{0.85}Mn_{0.15}$ samples, (compare Tables III and IV). A convincing demonstration (Fig. 4b) can be made that the ASRO observed in $Pd_{0.86}Ti_{0.14}$ is based on a Cu_3Au like structure – even allowing for the disagreements over palladium–titanium ordered phases evident from the phase diagrams. The ASRO in the $Pd_{0.85}Mn_{0.15}$ alloy appears to be based on an equiatomic ordered structure which is an analogue of the Type 3 (AF3) antiferromagnetic structure. This long range ordered structure does not exist in any known phase diagram, according to Clapp and Moss [30]. It is however the AB equivalent of the A_3B–DO_{22} superlattice of Ni_3V and Pd_3V. The AF3 structure is often called the "improved AF1" type as it is simply derived from the latter type. The corollary to this is that the atomically ordered structure shown in Fig. 6 is simply derived from the CuAuI structure. It is not therefore surprising, in view of the wide range of stability of the various "equiatomic" structures in the palladium–manganese system [27] that the ASRO in palladium rich alloys could tend towards this relatively obscure but simple equiatomic ordered phase.

Acknowledgements

This work has been supported by the Science and Engineering Research Council. One of us (AMS)

acknowledges receipt of an Egyptian Government Grant.

References

1. F. A. LEWIS, "The Palladium–Hydrogen System", (Academic Press, London, 1967).
2. P. C. ABEN and W. G. BURGESS, *Trans Faraday Soc.* **58** (1962) 1984.
3. M. L. H. WISE, J. P. G. FAIR, I. R. HARRIS and J. R. HIRST, in Proceedings of Congré's Int L'hydrogéne dans les Mét Paris, (Science of Industrie, Paris, 1972) **1** 72.
4. S. D. AXELRODT and A. C. MAKRIDES, *J. Phys Chem* **68** (1964) 2154.
5. A. S. DARLING, in Proceedings of Symposium of Less Common Means of Separation (Institute of Chemical Engineers, London, 1963).
6. M. NORMAN and I. R. HARRIS, *J. Less Common Metals* **18** (1969) 333.
7. M. L. H. WISE, J. P. G. FAIR and I. R. HARRIS, *ibid.* **41** (1975) 115.
8. D. T. HUGHES and I. R. HARRIS, *ibid.* **61** (1978) 9.
9. J. EVANS, I. R. HARRIS and L. S. GUZEI, *ibid.* **64** (1979) 39.
10. J. EVANS, I. R. HARRIS and P. F. MARFIN, *ibid.* **75** (1980) 49.
11. J. EVANS, I. R. HARRIS and D. K. ROSS, *ibid.* **89** (1983) 407.
12. T. B. FLANAGAN, S. MAJCHRZAK and B. BARANOWSKI, *Phil. Mag.* **25** (1972) 257.
13. R. C. PHUTELA and O. J. KLEPPA, *J. Chem Phys* **75** (1981) 4095.
14. W. B. PEARSON, in "Handbook of Lattice Spacings and Structures of Metals and Alloys" (Pergamon Press, Oxford, 1967) 2.
15. K. LONSDALE (ed) "International Tables for X-ray Crystallography", (The Kynoch Press, Birmingham, 1962) 3.
16. G. E. BACON, "Neutron Diffraction" (Clarendon Press, Oxford, 1975).
17. B. MOSER, D. T. KEATING and S. C. MOSS, *Phys. Rev.* **175** (1968) 868.
18. N. COWLAM and A. M. SHAMAH, *J. Phys. F: Met. Phys.* **11** (1981) 27.
19. B. E. WARREN, "X-ray diffraction" (Addison Wesley, Reading, Massachusetts, 1969).
20. J. M. COWLEY, *Phys. Rev.* **77** (1950) 669.
21. A. W. DWIGHT, J. W. DOWNEY, and R. A. CONNER Jr, *Acta Crystallogr.* **14** (1961) 75.
22. A. T. ALDRED, *Trans. AIME* **224** (1962) 1082.
23. N. AHMED and T. J. HICKS, *J. Phys. F: Met. Phys.* **4** (1974) L124.
24. J. M. COWLEY, *J. Appl. Phys.* **21** (1950) 24.
25. A. PASKIN, *Phys. Rev.* **134A** (1964) 247.
26. R. P. ELLIOTT, "Constitution of Binary Alloys – First supplement" (McGraw Hill, New York, 1965).
27. W. G. MOFFATT, "The Handbook of Binary Phase Diagrams" (Genium, Schenectady, New York, 1981).
28. J. S. SMART, "Effective Field Theories of Magnetism" (W. B. Saunders, Philadelphia, 1966).
29. M. I. DARBY and P. J. WEBSTER, *AIP Conf. Proc.* **29** (1975) 418.
30. P. C. CLAPP and S. C. MOSS, *Phys. Rev.* **171** (1968) 754.

Received 18 September
and accepted 8 December 1986